Temporal chaos of soliton dynamics in the PDE model of long Josephson junctions

1993 J. Phys. A: Math. Gen. 26 4937

(http://iopscience.iop.org/0305-4470/26/19/025)

J. Phys. A: Math. Gen. 26 (1993) 4937–4949. Printed in the UK

Temporal chaos of soliton dynamics in the PDE model of long Josephson junctions

G Filatrella† and G Rotoli‡
Department of Physics, University of Salerno, I-84081 Baronissi (SA), Italy

Received 8 June 1992, in final form 13 April 1993

Abstract. Calculations using the particle-map perturbative approach predict that fluxons in long Josephson junctions can exhibit chaotic motion when the junction is driven by an external microwave signal, applied to the Junction via magnetic field boundary conditions. The chaotic state is reached through a Feigenbaum-like cascade in the fluxon times of flight across the junction, with increasing signal amplitudes. In the present work the existence of such chaotic dynamics is demonstrated via numerical integration of the full perturbed sine–Gordon partial differential equation (PDE) model of the junction. The salient characteristics of the PDE dynamics are compared with the results obtained from the perturbative map approach. The resulting PDE chaos appears to be strictly low-dimensional: fluxons retain their shape without loss of spatial coherence, but their temporal motion is chaotic.

1. Introduction

In this paper we will examine the occurrence of chaos in a long Josephson Junction (LJJ) biased with both DC and RF terms. The subject was investigated in a previous paper [1] mostly by means of a simplified approach, called 'map approach'; our present purpose is to address it by modelling the LJJ with the complete partial differential equation (PDE) known as the perturbed sine–Gordon equation (PSGE) [2] governing the phase difference $\phi(x, t)$ between the two macroscopic wave functions of the superconducting films constituting the junction. We will address the problem to better ascertain the existence and features of this chaos mainly with simulations of the complete PDE equation. The question is relevant because relatively few PDE systems show direct evidence of low-dimensional chaos (see Abdullaev [3] for a review of the subject); among these we recall for the PSGE (in different dynamic regimes) the works of Soerensen *et al* [4] and of Taki *et al* [5]. The findings of Soerensen *et al* on the intermittence between Fiske steps have been explained in [6] as due to the competition between two incommensurate frequencies. The work of Taki *et al* [5], as the pioneering work of Bishop *et al* [7], is devoted to the study of the breather dynamics. Here we focus our attention on the kink dynamics for two reasons: (i) they are of more experimental relevance, and (ii) since the kink is a topological excitation it is easier to distinguish from other dynamic states. A secondary purpose is the comparison of the PDE results with the perturbative studies we have already published [1] of the very same model to establish the limits of the simplified approach. The advantage of the perturbative

† Present address: Physikalisches Institut, Lehrstuhl Experimentalphysik II, Universität Tübingen, D-72076 Tübingen, Federal Republic of Germany.

‡ Present address: Department of Energetics, University of L'Aquila, I-67100 Monteluco di Roio, L'Aquila, Italy.

0305-4470/93/194937+13$07.50

method is the reduction to a bi-dimensional map (see [8] for a complete discussion; an alternative more general version has been developed by Malomed [9]). Consequently, its computational cost is very low compared with the analysis of the complete system with (in principle) an infinite number of degrees of freedom. The two previous purposes are not independent: to use the perturbative approach we hypothesize that the solution of the PSGE is close enough to the single soliton solution of the unperturbed equation, i.e. it is low dimensional. In this sense the success of the perturbative analysis is an indirect proof that the dynamics involve mainly a single soliton-like solution.

There is also a practical motivation for the study of this problem: long Josephson junctions have been proposed as local oscillators for millimetre and submillimetre detectors [10]. In this case the essence of the device is based on the idea of a synchronous motion (phase locking) of the fluxon with the external microwave and consequently to detect the output power arising from the reflection of the fluxon at one edge. If the fluxon dynamics is destroyed such emission is destroyed too, while the loss of the phase locking would produce an undesirable growth of the noise of the signal.

The paper is organized as follows: in section 2 we give a description of the equation adopted as model of LJJ; in section 3 we report our fundamental results in terms of parameter space; in section 4 we analyse the strange attractors of the system and their dependence upon the parameters; in section 5 we study the problem of low dimensionality from the point of view of autocorrelation functions; some conclusions are collected in section 6.

2. Model

The long Josephson Junction [11] is defined by the fact that one spatial dimension of superconductive films making the junction is much longer than the so-called Josephson penetration depth λ_J. The electrical model leads to a $(1+1)$-dimensional nonlinear wave-propagation equation, known as the PSGE. In the so-called 'inline' configuration this equation reads

$$\phi_{xx} - \phi_{tt} - \sin\phi = \alpha\phi_t - \beta\phi_{xxt}\,. \tag{1}$$

We have in addition at the junction ends two time-dependant boundary conditions for a current biased junction (DC term) irradiated by a microwave field (AC term) [8]

$$\phi_x(0,t) + \beta\phi_{xt}(0,t) = -\chi + \eta(t) \tag{2a}$$

$$\phi_x(l,t) + \beta\phi_{xt}(l,t) = \chi + \eta(t)\,. \tag{2b}$$

In these formulas all the distances are normalized to λ_J, and times to $\omega_J^{-1} = \lambda_J/\bar{c}$, the inverse plasma frequency, where $\bar{c}$ is the speed of light in the junction. $\eta(t) = \eta_0 \sin\omega t$ is the normalized external magnetic field at the edges of the junction, α and β are loss parameters, χ is the normalized bias current supplied to the junction. The choice of the inline geometry was due to the fact that the motion of the fluxon inside the junction is purely ballistic since the currents are fed only through the edges.

Several methods, both numerical and perturbative, have been devised to directly solve or to gain information about the solutions of (1). A general method for perturbed solitonic equations is to use the so-called collective coordinates approach in which exact solutions of the unperturbed equation are written in terms of slowly time dependant parameters [12]. Inserting these parametric solutions into the perturbed equation gives a set of ordinary differential equations (ODEs) for the evolution of the parameters (collective coordinates), in our case the velocity of the centre of mass of the single soliton solution. In the inline case

the ODE can be solved analytically yielding a two-dimensional map in terms of the fluxon energy and phase of the external AC signal at each reflection [13]. In this paper much more attention will be paid to the numerical solution of the complete PDE problem. A point that we need to clarify is how we identify the map variables in the PDE context, or how we have reduced the infinite degrees of freedom system to a single degree of freedom system. We are assuming that the motion is of a soliton-like nature, so we identify the position of the fluxon as the point where the time derivative of the phase, i.e. the instantaneous voltage, is significatively higher than the background giving well-defined instantaneous voltage peaks [1]. There is still a difficulty because in the map approach the energy of the fluxon is commonly used as a dynamic variable which, involving the computation of the time derivative of the position, suffers from a severe numerical error in the PDE approach.

We have therefore chosen the time-of-flight (TOF) of the fluxon between the $(k-1)$th and kth reflections as a new dynamic variable T_k: through equation (8) of [13] it can be related to the initial energy. The other variable is as usual the phase $\theta_k = \sin^{-1}(\eta(t)/\eta_0)$ of the external microwave at the reflection of the fluxon.

The algorithms and the approximations used are briefly described in the appendix.

3. Parameter space

As usual, the first problem was the choice of the parameters to be studied. In (1) six parameters appear, namely $\alpha, \beta, \chi, \eta_0, \omega, L$. For the loss parameters the choice was restricted between the interesting case where chaos occurs (low values of α and β) and the computational necessity to increase them to avoid extremely long transients. Simulations with $0 \leqslant \beta \leqslant 0.04$ (realistic values for currently used junctions [14]) have demonstrated that, using the magnetic field η_0 as control parameter, the first bifurcation changes less than 10% in the above range. This is not surprising since the bias current is relatively low ($\chi \simeq 0.5$): the β term is expected to play an important role only when the bias current is close enough to the Josephson current (2 in normalized units) [15]. The loss parameter α is then almost fixed for the reasons discussed above; nevertheless we have explored several values of α in the range $0.05 \leqslant \alpha \leqslant 0.3$, always finding a discrepancy with the map simulations (in the sense discussed for the β term) within an accuracy of 10%. In the end we have chosen to set $\beta = 0$ and $\alpha = 0.1$, in order to reduce the number of parameters. To avoid the choice of too complicated a parameter space we have also fixed the length of the junction at $L = 10$: much shorter junctions cannot be of course considered 'long' and much longer junctions are seldom used in practice because of fabrication difficulties. Once we have chosen the length the frequency is more or less fixed because the RF induced step has to be far enough both from the asymptotic frequency of the zero field step and from its bottom. Moreover, in the map approach there is only a weak variation of the stable region, as a function of the frequency ω, in the above region ($0.3 \leqslant \omega \leqslant 0.6$). However, there is an indeterminacy in the choice of ω since phase-locking can be obtained if the fluxon frequency is a subharmonic of the RF frequency; in general the phase-locking condition is, with obvious notation

$$\omega_{\text{fluxon}} = \frac{n}{m}\omega_{\text{RF}}. \tag{3}$$

In the map context the case $n = 1$ is the most studied, and it is the most interesting from an applicative point of view. Steps with $m = 1$ show instability toward bifurcation only when the amplitude of the applied signal is so large as to destroy the single fluxon dynamics in the PDE analysis [1], while in the case $m = 5$ the annihilation region extends almost to

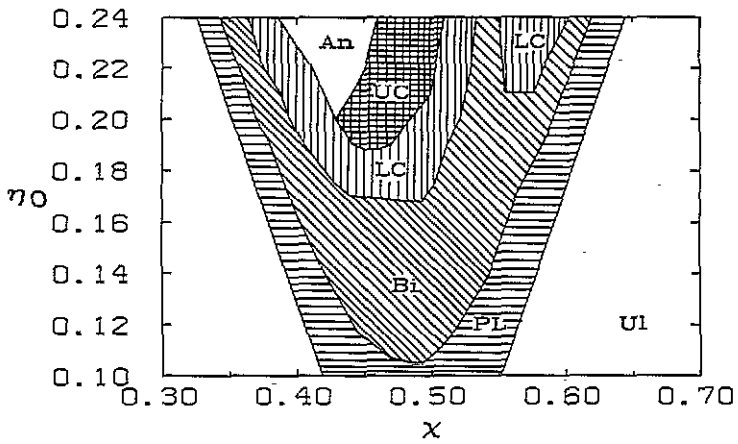

Figure 1. The parameter space in the PDE simulations. The parameters of the simulations are $L = 10$, $\alpha = 0.1$, $\beta = 0.0$, $\omega = 0.4$.

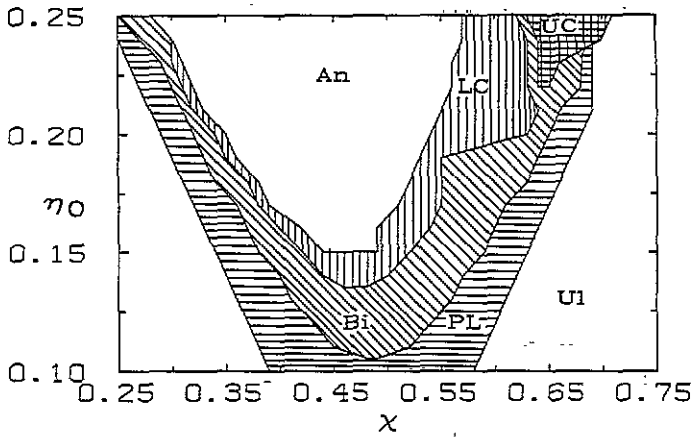

Figure 2. The parameter space in the map simulations. The parameters of the simulations are $L = 10$, $\alpha = 0.1$, $\beta = 0.0$, $\omega = 0.447411$.

$\eta_0 = 0$. Thus the choice of $m = 3$ is then almost the only possible to observe chaos. We have fixed $\omega_{RF}/3$ as the frequency of the fluxon without RF term at a DC bias $\chi \sim 0.485$. The map and PDE frequencies are slightly different due to the difference of the shape of the zero field step in the two cases, we are therefore forced to use two different values of the frequency for the two different approaches to keep the same bias current at the centre of the step. We parenthetically note that this choice is different from that used in [1] (where we used the same frequency but a different bias current) and greatly improves the agreement between the map and the PDE results. In conclusion we think that the study of the dynamics with variations of the two parameters η_0 and χ is the most interesting.

In figure 1 an overview of the parameter space studied with the PDE approach is presented; for comparison in figure 2 the prediction of the map approach is shown. Six regions are observed in both approaches. (i) The unlocked zone, UL, where the system is not locked to the external source, i.e. equation (3) is not satisfied for simple values of m and n. (ii) The phase locked region, PL, here the phase locking is realized in the simplest

way, one back-and-forth transit of the fluxon each three cycles of the external drive. (iii) The Feigenbaum-like cascade of bifurcation, Bi: in this region two-times-of-flight appear for each three RF cycles, followed by a period doubling cascade up to the beginning of chaos. The map prediction for the first bifurcation (see equations (44*a*) and (44*b*) of [8]) is confirmed by these numerical simulations. (iv) The voltage locked chaotic region, LC: the chaos that appears in this region has a special feature. In a *local* sense it is completely chaotic: the fluxon moves around in the T–θ phase plane without any possible prediction, but in a *global* sense it is ordered because the average of the time-of-flight is still locked to the external drive. This was confirmed to four digits of accuracy. (v) The voltage unlocked chaotic region, UC: here any memory of the external drive is lost, and the average of the times of flight converges to a different value.; (vi) The annihilation region, An: in this region fluxon dynamics cannot develop [1].

It can be noticed that the functional behaviour between the map and the PDE approach seems to be the same. An important point is that in both the cases the instabilities first occur *at the middle* of the step, where the free running frequency of the fluxon exactly satisfies the phase locking conditions, so that we cannot speak of a competition between two frequencies, as in the case of short junctions [16]. A similar interpretation has also been given in [6] for intermittence between Fiske steps.

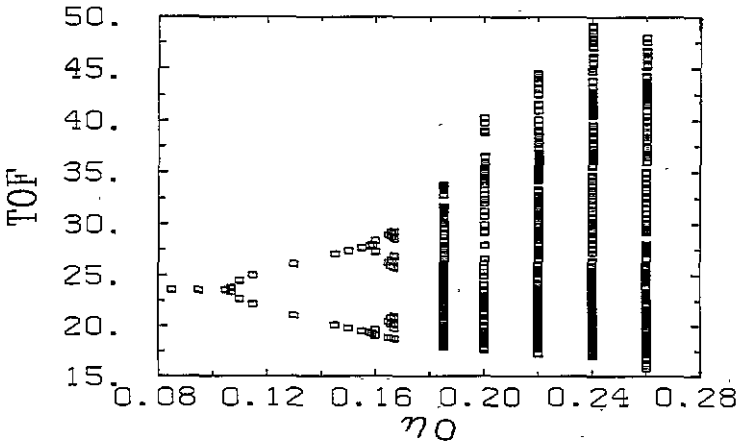

Figure 3. Bifurcation tree for the PDE simulations. Parameters are $L = 10$, $\alpha = 0.1$, $\beta = 0.0$, $\omega = 0.4$; $\chi = 0.485$.

In figure 3 the detailed dynamics fixing $\chi = 0.485$ and varying η_0 for the same parameters of figure 1 is shown. The technique used was to adiabatically increase the magnetic field until a desired value was reached. Adiabatically here means that the system has relaxed to a steady state as has been proved by halving the sweep velocity. The test that the system has achieved a steady state is trivial when the motion is periodic; however, caution should be used when we claim that the dynamics is chaotic. For the moment let us use an heuristic definition of chaos as 'non-evidently convergent to a periodic solution'; a more accurate analysis will be carried out in a next section. To simplify the representation we plot only the TOF, T_k, i.e. one of the two degrees of freedom used in the map approach. An analogous figure could be obtained using the other degree of freedom, the phase θ_k.

The bifurcation tree seems very similar to those obtained with the map approach [8]. Note that to the eye there is no difference in the transition from the voltage locked chaos to the unlocked region (which occurs at about $\eta_0 = 0.190$). The Feigenbaum ratio is 6.1 for the

fourth bifurcation, in good agreement with the value of 5.9 found for the case $\beta \neq 0$ [17].

4. Strange attractors

The dynamics of the fluxons has been observed also plotting both the variables θ_k and T_k to find the strange attractors in the phase plane. Figure 4 shows how the strange attractors are modified by the bias current, as we will discuss below. We have evaluated the fractal dimensions of the strange attractors using the Grassberger–Procaccia algorithm [18]. For $\chi = 0.485$, $\eta = 0.170$ (the other parameters are the same as in figure 1), i.e. in the LC region, we have found the dimension to be 1.1, close to the result obtained by a box counting in the map approach [1]. Increasing the magnetic field up to $\eta = 0.200$ (in the UC region) the dimension was in turn found to be 1.3. The estimate is rough because of the relatively small number of points employed (3×10^3). It is worthwhile to note that PDE attractors appear very similar to map attractors at least for low values of η_0 (typically in the LC region) [19]. An independent estimate of fractal dimension of attractors will be given in the following section.

Figure 5 shows the I–V curve computed for two different values of the magnetic field, in the LC (curve a) and UC (curve b) regions, respectively. Clearly evident in the middle of the UC step is the loss of voltage locking. This phenomenon has a dynamical counterpart in the attractors of figure 4(a)–(c); in figure 4(a) an attractor in the LC region is shown, in the remaining parts unlocked attractors are shown.

In figure 4(a) we have a compact 'tail' structure in the region of higher TOF with no TOF longer than 35. In figure 4(b) the current was decreased to $\chi = 0.470$; here we note, as a sign of entering in the UC region, a change in the attractor: the partial disruption of the previous tail structure in which new long TOF develop. These phenomena reach the maximum in figure 4(c) where $\chi = 0.445$ and the longest TOF are developed. It is difficult to decide if so long TOF can be ascribed to an effective change of tails structure or if those tails exist also in the LC region but, being seldom visited, have not yet appeared in the simulations (i.e. in the first 800 TOF). However, the difference between the two figures is evident so we can speak of qualitative change between LC and UC attractors.

A justification for this behaviour can be found noting that at about $\chi = 0.470$ TOF become sufficiently long to 'catch' the $m = 5$ subharmonic whose phase-locking TOF is $\simeq 39.0$. This seems to indicate that in the UC region the system shows competition between two different attractors. Further evidence of this is provided by the following observations.

(a) The basins corresponding to the subharmonic $m = 3$ and $m = 5$ can overlap. The perturbative approach predicts the range of existence of phase lock: $m = 3$ and $m = 5$ subharmonics steps extend from $\chi = 0.484 - \eta_0$ to $\chi = 0.484 + \eta_0$ and from $\chi = 0.364 - \eta_0$ to $\chi = 0.364 + \eta_0$ respectively. Thus for the same current $\chi = 0.470$ we can have two different attractors.

(b) PDE simulations show the possibility, biasing the junction at a bias value $\chi = .485$, of reaching the $m = 5$ subharmonic from the $m = 3$ state by slightly increasing η_0 from 0.190 to 0.195: the system falls on the $m = 5$ attractor developing a two-TOF state. We note also that the stability analysis [8] indicates that the $m = 5$ basin for such a value of the bias and of the magnetic field does not contain a chaotic attractor.

(c) The average voltage is moved to a lower value with respect to the $m = 3$ attractor, i.e. closer to the $m = 5$ average voltage supporting the idea that the system visits both the attractors. In the map data UC region is in a different region *above* the centre of the step, and the average voltage is moved to a *higher* value ($\simeq 10\%$ more than the phase-locked value), closer to the $m = 2$ attractor. Overlap should then take place with the $m = 2$

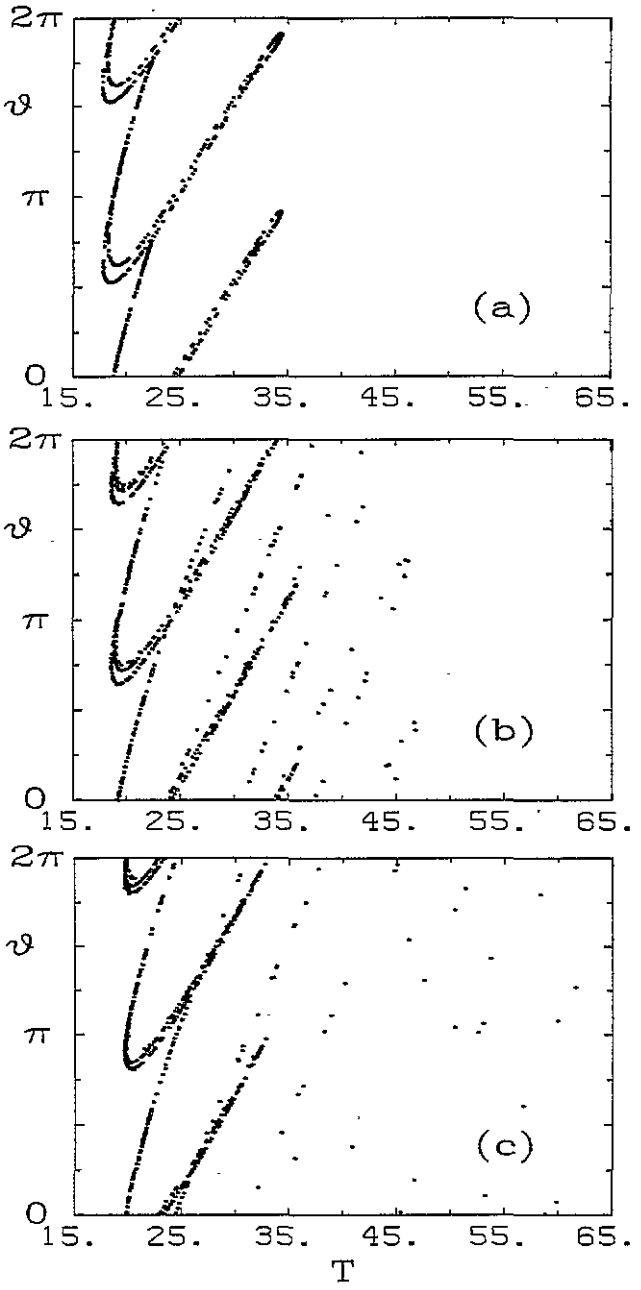

Figure 4. Chaotic strange attractors. The parameters of the simulations are $L = 10$, $\alpha = 0.1$, $\beta = 0.0$, $\omega = 0.4$, the DC and RF bias current are (*a*) $\chi = 0.493$, $\eta_0 = 0.150$, (*b*) $\chi = 0.470$, $\eta_0 = 0.150$, (*c*) $\chi = 0.445$, $\eta_0 = 0.150$.

attractor, for the very same reasons discussed in point (a).

On the other hand an exploration of the phase space with different initial conditions has not revealed the contemporary presence of stable attractors. Thus for different values of χ and η_0 the system can develop some 'intermittence' between $m = 3$ and $m = 5$ (and in principle with all higher subharmonic when the TOF are sufficiently sparse). This mechanism probably drives the system out of the $m = 3$ LC state because higher subharmonics correspond to different voltages. This mechanism can simply destroy the fluxon, as happens

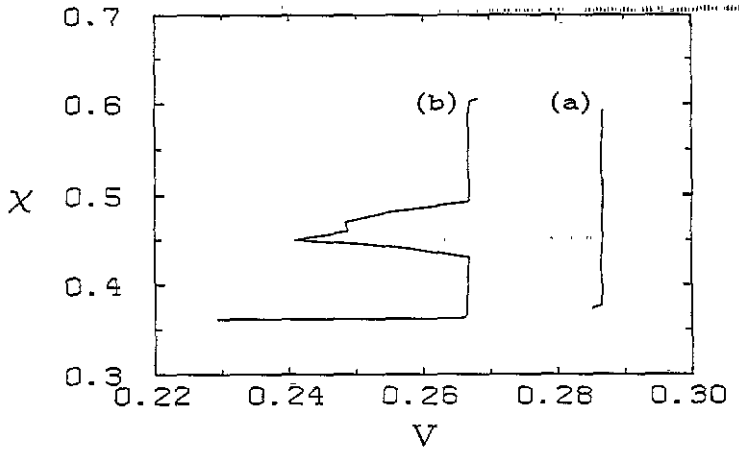

Figure 5. The I–V characteristic when the system shows (a) locked, and (b) unlocked chaos. The parameters of the simulations are $L = 10$, $\alpha = 0.1$, $\beta = 0.0$, $\omega = 0.4$, and $\eta_0 = 0.175$ and $\eta_0 = 0.190$ for (a) and (b), respectively. Step (a) has been offset by $V = 0.02$ to improve readibility.

for higher η_0 in the An region, driving the system into attractors, very unstable, that lead to the annihilation of the fluxon. Obviously the limitation of subharmonics involved is essentially due to fact that: (1) only for the few first subharmonics can the basins effectively overlap in chaotic regimes, and (2) higher subharmonics are progressively more unstable; being mainly chaotic they develop a large reciprocal instability and a large instability toward the annihilation.

5. Autocorrelation

Since we have claimed to study in which measure the dynamics of the system is low dimensional we will now try to make quantitative our assertion. To demonstrate that during the dynamics the phase $\phi(x,t)$ shows a markedly correlated behaviour in space we have computed the spatial mean autocorrelation

$$F(x) = \frac{1}{T}\int_0^T \mathrm{d}t \left\langle \phi_t(x+x',t)\phi_t(x',t)\right\rangle \tag{4}$$

We expect that for a localized soliton-like solution the autocorrelation should be significatively different from zero only over a length of λ_J, while for turbulent motion it should be more or less flat [20]. The time counterpart of these assertions is that the temporal mean autocorrelation

$$F(t) = \frac{1}{L}\int_0^L \mathrm{d}x \left\langle \phi_t(x,t+t')\phi_t(x,t')\right\rangle \tag{5}$$

should show a highly correlated behaviour in correspondence of the average TOF during the periodic motion and a tendency toward a flat behaviour with the onset of chaos. This is what we effectively observe in figure 6. In figure 6(a) are reported three curves corresponding to the spatial mean autocorrelation in the PL, Bi and UC regions; the temporal mean autocorrelation for the same regions is respectively shown in figure 6(b)–(d). It seems evident that the drastic change in the temporal evolutions does not affect significatively

the first quantity, which always shows a correlation over distance of λ_J, while the time autocorrelation reflects a sharp change between the periodic and the chaotic regimes. This is evidently related to the well known phenomenon of noise-rise in chaotic spectra to which we return in the next section.

The problem as to whether the presence of the soliton-like dynamics has to be interpreted as chaotic or not has also been investigated by means of the Lyapunov exponents. In [1] we have evaluated the Lyapunov exponents for the map approach finding typical positive exponents in the chaotic region. It is clear that also TOF of PDE can be thought as a time series coming from a 'map': this corresponds to a projection of the full ∞-dimensional dynamics on a two-dimensional phase space. Evaluation of Lyapunov exponents of the projected system is possible, but we can not expect substantial differences from the map approach because it is obvious that in this way we consider the PDE as a low-dimensional system *a priori*. A somewhat different analysis can be carried out that takes into account all degrees of freedom of the PDE system, interpreting the discrete version of (1) (see the appendix) as the evolution of an N-dimensional vector [21]. We have then evaluated the first N_L Lyapunov exponents with the method of Benettin *et al* [22] following the evolution of an N_L-dimensional volume under phase flux generated by equation (1). The general behaviour of such exponents can be summarized in the following points: (i) they are independent of N within the chosen limit on their convergence (here N indicates the number of sections into which the LJJ is divided to integrate (1)—see the appendix for typical values); (ii) they are independent of N_L; (iii) all the exponents are negative below $\eta_0 = 0.168$, i.e. before the chaos sets in; (iv) the maximum exponent is the only positive exponent in the chaotic regions. Both points (ii) and (iv) are *strongly indicative of the low dimensionality of full* PDE dynamics. Moreover, numerical values are consistent with the previous estimate of fractal dimension, according to the Kaplan–Yorke conjecture [18]. We found for $\eta_0 = 0.170$ the following values of first two Lyapunov exponents: $\lambda_1 = 0.0150$ and $\lambda_2 = -0.0478$; and from this Kaplan–Yorke fractal dimension is found to be 1.313. Next for $\eta_0 = 0.200$ the exponents are: $\lambda_1 = 0.0320$ and $\lambda_2 = -0.0469$, which give 1.682 for the (Kaplan–Yorke) fractal dimension. As pointed out in section 4 the direct evaluation of the fractal dimension gives 1.1 and 1.3 for $\eta_0 = 0.17$ and $\eta_0 = 0.20$, respectively. This is consistent with the fact that the Kaplan–Yorke conjecture gives an upper bound to the measure of the attractor [18].

A somewhat more practical point of view is that, for the practical purposes of fabricating a device, the only important feature is the linewidth of the emitted radiation. For such a scope the behaviour of the time derivative of the phase at the edges is of crucial importance from an experimental point of view because it is directly related to the signal emitted from the junction. In the PDE approach we can analyse the radiation emitted by the fluxon at each reflection $\phi_t(0, t)$ (the voltage at one edge). It has not been possible to evaluate exactly the linewidth of the radiation because it is much smaller than accuracy of the numerical scheme used here (the evaluation of such a narrow linewidth would require an *ad hoc* method such as that used by If *et al* [23]) and because we are neglecting thermal noise, but just to compare what relatively happens to the spectrum. This is indicated in figure 7(a) and 7(b), which show the Fourier transform of the edge voltage in the PL and UC regions, respectively. Both the noise rise and the depression of the power emitted at the fundamental frequency are evident, two phenomena highly undesirable for the fabrication of practical devices.

6. Conclusion

The nature of chaos in the PDE system seems to be really *low dimensional*, i.e. the whole system behaves in a way that can be well described by the two degrees of freedom of the

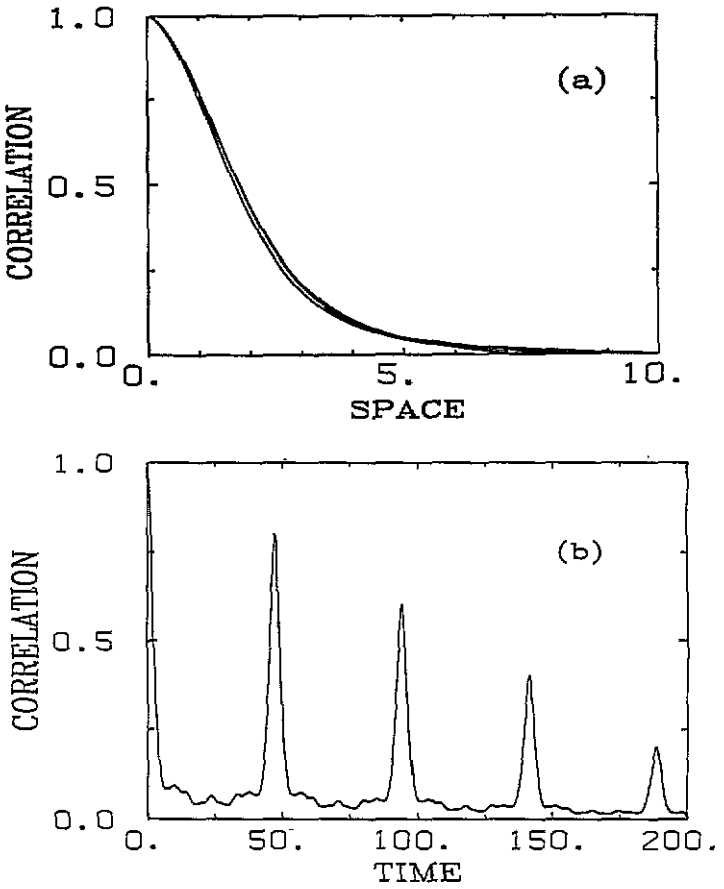

Figure 6. Spatial and temporal autocorrelation, equations (4)–(5): (*a*) spatial $\eta_0 = 0.100$, 0.150 and 0.190, respectively; (*b*) temporal for $\eta_0 = 0.100$; (*c*) temporal for $\eta_0 = 0.150$ and (*d*) temporal for $\eta_0 = 0.190$.

soliton-like solutions. The main argument in favor of the low-dimensional behaviour of the full PDE system is the finite dimension of the attractors obtained either by means of a straightforward estimate of the dimension and by means of the Lyapunov exponents (via the Kaplan–Yorke conjecture).

In particular the Lyapunov exponent estimate, being completely independent from any *a priori* projection of phase space, is a very powerful test of postulated low dimensionality.

Quantitative differences, such as the values of the control parameter for the occurrence of chaos or bifurcation and the Feigenbaum ratio, do not lead to qualitative discrepancies except for the phenomenon of the unlocked voltage chaos, but also in this zone the solitonic nature of the solutions seems to be well preserved.

These effects might be ascribed to the fact that the fluxon in the map formalism has no spatial extension; in the full model by contrast it has finite size. Consequently the external drive acts as a point-like excitation in the map approach and over a finite time in the PDE approach. This might lead to a different model of the underlying dynamics.

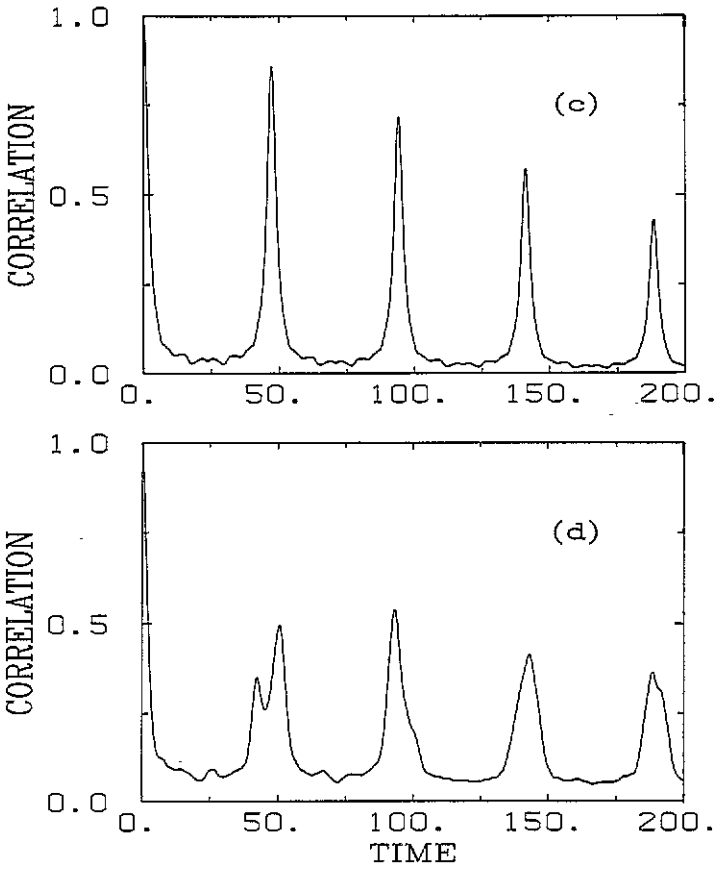

Figure 6. (Continued).

Acknowledgments

We wish to thank R D Parmentier for illuminating comments and for a critical reading of the manuscript. We had several discussions with G Costabile, R Monaco, S Pagano, M Salerno, and A C Scott, to whom we are most grateful.

Appendix. Algorithm for PDE solution

To solve (1) we have assumed instead that the function $\phi(x,t)$ is a discrete spatial variable, $\phi(i\Delta x,t)$. For the discrete system the operator $\partial^2/\partial x^2$ is substituted by

$$\frac{\partial^2}{\partial x^2} \to \frac{1}{\Delta x^2}[\phi_{i+1,j} - 2\phi_{i,j} + \phi_{i+1,j}] \qquad 2 \leqslant i \leqslant N-1 \tag{A1}$$

and the time equation for each point becomes

$$\frac{\mathrm{d}^2\phi_i}{\mathrm{d}t^2} = \gamma - \alpha\frac{\mathrm{d}\phi_i}{\mathrm{d}t} - \sin\phi_i + \frac{1}{\Delta x^2}[\phi_{i+1} - 2\phi_i + \phi_{i+1}] + \frac{\beta}{\Delta x^2}\frac{\mathrm{d}}{\mathrm{d}t}[\phi_{i+1} - 2\phi_i + \phi_{i+1}]. \tag{A2}$$

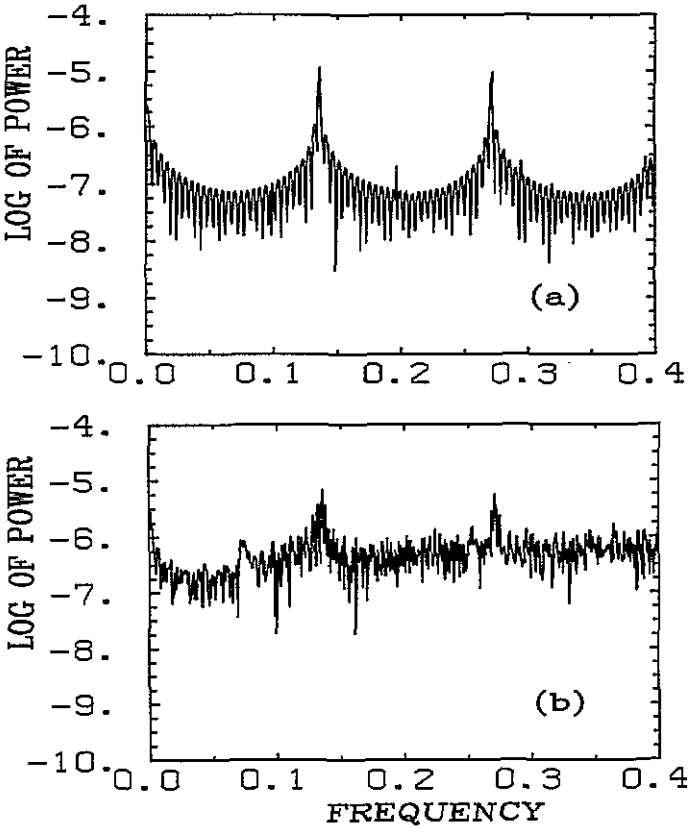

Figure 7. Spectrum of the emitted signal at the right-hand side. The parameters of the junction are $L = 10$, $\alpha = 0.1$, $\beta = 0.0$, $\omega = 0.4$. (*a*) $\eta_0 = 0.100$, $\chi = 0.485$; (*b*) $\eta_0 = 0.190$, $\chi = 0.445$.

At the extreme to take into account boundary conditions one adds two virtual points ($i = 0$ and $i = N + 1$) and replaces the operator $\partial/\partial x$

$$\frac{\partial}{\partial x} \to \frac{1}{2\Delta x}\left[\phi_{i+1} - \phi_i\right]. \tag{A3}$$

Boundary conditions are written as

$$\phi_0 + \beta\frac{\mathrm{d}\phi_0}{\mathrm{d}t} = \phi_1 + \beta\frac{\mathrm{d}\phi_1}{\mathrm{d}t} - 2\eta(t)\Delta x \tag{A4}$$

$$\phi_{N+1} + \beta\frac{\mathrm{d}\phi_{N+1}}{\mathrm{d}t} = \phi_N + \beta\frac{\mathrm{d}\phi_N}{\mathrm{d}t} + 2\eta(t)\Delta x\,. \tag{A5}$$

In this way the PDE system is transformed into N coupled ordinary differential equations that can be solved numerically. To check that, for a sufficiently small step size, the results are independent of the discretization chosen for the spatial derivative we have also used a five-point discretization for the operator $\partial^2/\partial x^2$

$$\frac{\partial^2}{\partial x^2} \to \frac{1}{12\Delta x^2}\left[-\phi_{i+2} + 16\phi_{i+1} - 30\phi_i + 16\phi_{i-1} - \phi_{i-2}\right] \qquad 2 \leqslant i \leqslant N-2. \tag{A6}$$

We have again used the three-point discretization for points $i = 1$ and $i = N + 1$. The two schemes converge, for sufficiently small step size, to the same results. The computational

efficiencies of the two schemes are not significatively different. Time evolution was in turn computed numerically with two different tools: a second-order predictor–corrector, and a Bulirsh-Stoer algorithm; again we have not found any discrepancy between the solutions within the given accuracy (10^{-4} on TOF). The typical CPU time was estimated to be 20 hours for each 1000 TOF on a VAX 6400, with $N = 120$. Runs have been made also with $N = 60$ and $N = 240$ to test the independence of N. Lyapunov exponents were evaluated with $N_L = 1, 2, 4, 8, 16$.

References

[1] Rotoli G and Filatrella G 1991 *Phys. Lett.* **156A** 211
[2] Parmentier R D 1978 *Solitons in Action* ed K Lonngren and A C Scott (New York: Wiley) p 173
[3] Abdullaev F Kh 1989 *Phys. Rep.* **179** 1
[4] Soerensen M P, Arley N, Christiansen P L, Parmentier R D and Skovgaard O 1983 *Phys. Rev. Lett.* **51** 1919
[5] Taki M, Spatschek K H, Fernandez J C, Grauer R and Reinisch G 1989 *Physica* **40D** 65
[6] Zheng D J, Yeh W J and Symko O G 1989 *Phys. Lett.* **140A** 225
Yeh W J, Symko O G and Zheng D J 1990 *Phys. Rev.* B **42** 4080
[7] Bishop A R, Lomdahl P S, Kerr W C, Williams H B and Trullinger S E 1983 *Phys. Rev. Lett.* **50** 1095
[8] Salerno M, Samuelsen M R, Filatrella G, Pagano S and Parmentier R D 1990 *Phys. Rev.* B **41** 6641
[9] Malomed B A 1990 *Phys. Rev.* B **41** 2037
[10] Monaco R, Pagano S and Costabile G 1987 *Phys. Lett.* A **124** 523
[11] Barone A and Paterno G 1982 *Physics and Applications of the Josephson Effect* (New York: Wiley)
[12] McLaughlin D W and Scott A C 1978 *Phys. Rev.* A **18** 1652
[13] Filatrella G, Rotoli G and Parmentier R D 1990 *Phys. Lett.* **148A** 122
[14] Costabile G, Monaco R, Pagano S and Rotoli G 1990 *Phys. Rev.* B **42** 2651
[15] Davidson A, Pedersen N F and Pagano S 1986 *Appl. Phys. Lett.* **48** 1306
[16] Kautz R L and Monaco R 1985 *J. Appl. Phys.* **57** 875
[17] Rotoli G and Filatrella G 1991 *Proc. of the VII Interdisciplinary Workshop on Nonlinear Coherent Effects in Physics and Biology* ed M Peyrard and M Remoissenet (Berlin: Springer) p 284
[18] Grassberger P and Procaccia I 1983 *Physica* **9D** 189
[19] Filatrella G, Grønbech-Jensen N, Monaco R, Pagano S, Parmentier R D, Pedersen N F, Rotoli G, Salerno M and Samuelsen M R 1991 *Proc. Workshop on Nonlinear Superconductivity Electronics and Josephson Devices* ed G Costabile, S Pagano, N F Pedersen and M Russo (New York: Plenum) p 253
[20] Octavio M 1984 *Phys. Rev.* B **29** 1231
[21] Caravati G, Giorgilli A and Galgani L 1983 *Lettere Nuiovo Cimento* **38** 385
[22] Benettin G, Galgani L, Giorgilli A and Strelcyn J M 1980 *Meccanica* **15** 9
[23] If F, Christiansen P L, Parmentier R D, Skovgaard O and Soerensen M P 1985 *Phys. Rev.* B **32** 1512